Applied Mathematics & Information Sciences
An International Journal

Effect of Induced Magnetic Field on Peristaltic Transport of a nanofluid in an asymmetric channel: Closed form Solution

Khalid Nowar*

Department of Mathematics, King Saud University, P. O. Box 2455, Riyadh 11451, Saudi Arabia

Abstract: In this paper, the problem of peristaltic transport of a nanofluid in an asymmetric channel under the effect of induced magnetic field has been investigated theoretically. The problem is simplified under the assumption of long wave length and law Reynolds number. Exact analytic solutions for the present problem are obtained. Expressions for the velocity, stream function, temperature distribution, nanoparticles concentration, pressure gradient, pressure rise, magnetic force function, axial magnetic field, and current density distribution are computed. The effect of various emerging parameters on the flow characteristic are shown and discussed. The trapping phenomena have been also discussed. Results show that the magnitude of the velocity decreases in the center of the channel while it increases near the channel wall with an increase in Hartmann number M. It is also noted that the size of the trapped bolus increases in the lower half of the channel when we increase the Hartmann number as well as the local Grashof number.

Keywords: Peristalsis, Induced magnetic field, Nanofluid, Asymmetric channel, Grashof number

1 Introduction

It is well known that nanofluids are nanometer-sized particles, which is called nanoparticles. These fluids are engineered colloidal suspensions of nanoparticles in a base fluid. The nanoparticles used in nanofluids are made of metals (Al, Cu), oxides (Al_2O_3), carbides (SiC), nitrides (AlN, SiN) or nonmetals (Graphite, carbon nanotubes) and the base fluid is usually a conductive fluid, such as water or ethylene glycol. Nanofluids have novel properties that make them potentially useful in many applications in heat transfer, including microelectronics, fuel cells, pharmaceutical processes, and hybrid-powered engines. In engineering devices it has been widely used for engine cooling/vehicle thermal management, domestic refrigerator, chiller, heat exchanger, and nuclear reactor, in grinding, in machining, in space, defense and ships, and in boiler flue gas temperature reduction. Nowadays, there is a focus of the researchers in the flow analysis of nanofluids due to the fluids enhance thermal conductivity of the base fluid enormously, which is beyond the explanation of any existing theory. Furthermore are very stable and have no additional problems, such as

sedimentation, erosion, additional pressure drop, etc. See for example refs. [1]-[10].

Recently, the MHD peristaltic flow of electrically conducting fluids have received a great attention of many researchers [11]-[20]. This is due to its different applications in medical sciences and bioengineering. The MHD characteristics are important in understanding some practical phenomena such as blood pump machine, Magnetic resonance imaging (MRI) which is used for diagnosis of brain, cancer tumor treatment, vascular diseases, hyperthermia, and blood reduction during surgeries. It has been noticed that there are numerous attempts of researchers to study MHD peristaltic transport in the presence of uniform magnetic field, but no much attention has been given to the peristaltic flows with an induced magnetic field. Since the first attempt by Vishnyakov and Pavlov [21] by considering Newtonian fluids. Later, Mekheimer [22] studied the MHD flow of a conducting couple stress fluid in a symmetric channel. Mekheimer et al [23] examined the peristaltic flow of a magneto-micropolar fluid under the effect of induced magnetic field. Hayat et al [24] addressed the effect of induced magnetic field on peristaltic transport of a third

* Corresponding author e-mail: khalidnowar@yahoo.com

order fluid. The effect of induced magnetic field on peristaltic flow of a Carreau fluid had been also investigated by Hayat et al [25].

In the past few years, Y. Abd elmaboud [26] studied the influence of induced magnetic field on peristaltic flow. Akram et al [27] obtained numerical and analytical solutions for peristaltic flow of a Williamson fluid in the occurrence of induced magnetic field. Akram and Nadeem [28] investigated the influence of induced magnetic field and heat transfer on the peristaltic flow of a Jeffrey fluid. M. Mustafa et al [29] investigated the effects of induced magnetic field on the mixed convection peristaltic motion of nanofluid in a vertical channel considering a non-uniform motion where they took the velocity gradients into account and the viscous stress occurs in the governing equations of motion and consequently the solutions they obtained are approximated. In this work we considered the influences of induced magnetic field on peristaltic flow of a nanofluid in a horizontal asymmetric channel by considering that the motion is uniform, i.e. there are no velocity gradients, in this case the rates of strain disappear and hence the viscous stresses also disappear. Neglecting velocity gradients enables us to obtain closed form solutions to our problem.

The present paper is organized as follows. Section 3 contains the formulation of the problem. In section 4 the rate of volume flow. section 5 presents the solution of the problem under consideration. Section 6 deals with the results. Discussion, and trapping phenomenon. The conclusions have been summarized in Section 7.

2 Problem formulation

We aim at considering the peristaltic flow of an incompressible viscous electrically conducting nanofluid in a two dimensional infinite asymmetric channel of width $d_1 + d_2$. Asymmetry in the channel is produced by assuming the peristaltic wave trains propagating with constant speed c along the walls to have different amplitudes and phases. The shapes of the channel walls are presented as:

$$H_1(X,t) = d_1 + a_1 \cos(\frac{2\pi}{\lambda}[X - ct]), \text{Upper wall}, \quad (1)$$

$$H_2(X,t) = -d_2 - a_2 \cos(\frac{2\pi}{\lambda}[X - ct] + \phi), \text{Lower wall}, \quad (2)$$

where a_1, a_2 are the amplitudes of the upper and lower waves, λ is the wave length, c is the velocity of propagation, t is the time, X is the direction of wave propagation, ϕ is the phase difference and varies in the range $0 \leq \phi \leq \pi$, note that $\phi = 0$ corresponds to an asymmetric channel with waves out of phase and $\phi = \pi$

describes the case where waves are in phase. Further, d_1, d_2, a_1, a_2, and ϕ satisfy the following inequality,

$$a_1^2 + a_2^2 + 2a_1a_2 \cos\phi \leq (d_1 + d_2)^2. \quad (3)$$

so that the walls will not intersect with each other. We choose cartesian coordinates system for the channel with X along the center line of the channel and Y is transverse to it. A constant magnetic field of strength H_0 acting in the transverse direction results in an induced magnetic field $\mathbf{H}(h_x(X,Y,t), h_Y(X,Y,t), 0)$. The total magnetic field thus is $\mathbf{H}^+(h_x(X,Y,t), H_0 + h_Y(X,Y,t), 0)$. Denoting the velocity components U and V along the X and Y directions respectively in the fixed frame, the velocity field is $V = (U(X,Y,t), V(X,Y,t), 0)$. The transformation from laboratory frame of reference (X,Y) to wave frame of reference (x,y) is given by

$$x = X - ct, \ y = Y, \ u = U - c, \ v = V, \text{ and } \ p(x) = P(x,t), \quad (4)$$

where (u,v), p and (U,V), P are the velocity components and pressure in the wave and fixed frames of reference respectively.

The governing equations of motion for the present flow are (see [22] and [29])
(I) The Maxwell's equations

$$\nabla.\mathbf{H} = 0, \ \ \nabla.\mathbf{E} = 0, \quad (5)$$

$$\nabla \times \mathbf{H} = \mathbf{J}, \ \ \mathbf{J} = \sigma[\mathbf{E} + \mu_e(\mathbf{V} \times \mathbf{H})], \quad (6)$$

$$\nabla \times \mathbf{E} = -\mu_e \frac{\partial \mathbf{H}}{\partial t}, \quad (7)$$

(II) The continuity equation

$$\nabla.\mathbf{V} = 0, \quad (8)$$

(III) The momentum equation

$$\rho_f \frac{d\mathbf{V}}{dt} = -\nabla P + \mu \nabla^2 \mathbf{V} + \mu_e(\mathbf{H}^+ . \nabla)\mathbf{H}^+ - \frac{\mu_e}{2}\nabla\mathbf{H}^{+2} + \mathbf{f}, \quad (9)$$

(IV) The equation of nanofluid temperature

$$(\rho c')_f \frac{dT}{dt} = k\nabla^2 T + (\rho c')_p[D_B \nabla C \nabla T + (D_T/T_0)\nabla T \nabla T], \quad (10)$$

(V) The nanoparticle volume fraction phenomena

$$\frac{dC}{dt} = D_B \nabla^2 C + (D_T/T_0)\nabla^2 T, \quad (11)$$

(VI) The induction equation

$$\frac{\partial \mathbf{H}^+}{\partial t} = \nabla \times (V \times \mathbf{H}^+) + \frac{1}{\zeta}\nabla^2 \mathbf{H}^+, \quad (12)$$

where, μ_e is the magnetic permeability, ρ_f is density of the fluid, $\frac{d}{dt}$ is the material derivative, μ is viscosity of the
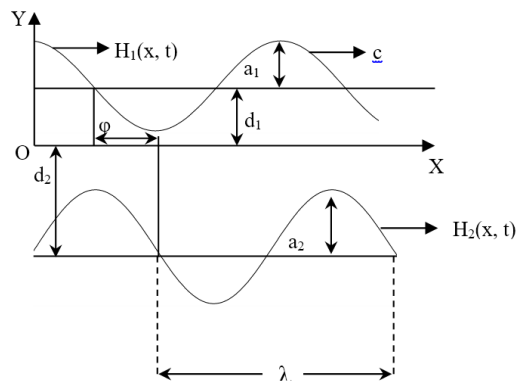
Fig. 1: Geometry of the problem.

Fig. 2: Variations of velocity profile u with y for various values of Hartmann number M (panel **a**), local Grashof number G_r (panel **b**), amplitude of upper wave a (panel **c**), and width of the channel d (panel **d**). The other parameters chosen are: $F = 2, x = 1, d = 1, a = 0.3, b = 0.7, N_b = 0.8, N_t = 0.5, \phi = 0.2, G_r = 0.5, B_r = 0.5$ (panel **a**); $F = 2, x = 1, d = 1, a = 0.3, b = 0.7, N_b = 0.8, N_t = 0.5, \phi = 0.2, M = 1, B_r = 0.5$ (panel **b**); $F = 2, x = 1, d = 1, M = 1, b = 0.7, N_b = 0.8, N_t = 0.5, \phi = 0.2, G_r = 0.5, B_r = 0.5$ (panel **c**); $F = 2, x = 1, M = 1, a = 0.3, b = 0.7, N_b = 0.8, N_t = 0.5, \phi = 0.2, G_r = 0.5, B_r = 0.5$ (panel **d**).

fluid, ∇^2 is laplacian operator, t is the time, $(\rho c')_f$ is the heat capacity of base fluid, $(\rho c')_p$ is the effective heat capacity of the particles material, c' is the volumetric volume expansion coefficient, C is the nanoparticle volume fraction, T is the dimensional nanoparticle temperature, T_0 is fluid mean temperature, D_B is the brownian diffusion coefficient and D_T is the thermophoretic diffusion coefficient.

To describe the fluid flow in a non-dimensional form we define the following quantities

$$x^* = \frac{x}{\lambda}, y^* = \frac{y}{d_1}, u^* = \frac{u}{c}, v^* = \frac{v}{c}, h_1 = \frac{H_1}{d_1}, h_2 = \frac{H_2}{d_1},$$

$$\delta = \frac{d_1}{\lambda}, R_e = \frac{\rho d_1 c}{\mu}, t^* = \frac{c}{\lambda}t, v = \frac{\mu}{\rho_f}, p^* = \frac{pd_1^2}{c\lambda\mu}, b = \frac{a_2}{d_1},$$

$$d = \frac{d_2}{d_1}, a = \frac{a_1}{d_1}, \alpha = \frac{k}{(\rho c')_f}, \theta = \frac{T - T_0}{T_1 - T_0}, \Omega = \frac{C - C_0}{C_1 - C_0},$$

$$N_b = \frac{\rho c'_p D_B (c_1 - c_0)}{(\rho c')_f \alpha}, N_t = \frac{\rho c'_p D_T (T_1 - T_0)}{(\rho c)_f \alpha T_0},$$

$$G_r = \frac{\alpha g (T_1 - T_0) d_1^2}{vc}, B_r = \frac{\alpha g (C_1 - C_0) d_1^2}{vc}, Pr = \frac{v}{\alpha},$$

$$S = \frac{H_0}{C} \sqrt{\mu_e / \rho_f}, \Phi = \frac{\Phi}{H_0 d_1}, p_m = p + \frac{1}{2} R_e \delta \frac{\mu_e H^{+2}}{\rho_f c^2}$$

$$R_m = \sigma \mu_e c d_1, h_X = \Phi_Y, h_Y = -\Phi_X, \quad (13)$$

where R_e is the Reynolds number, δ is the dimensionless wave number, v is the dynamic viscosity parameter, P_r is the Prandtl number, N_b is the Brownian motion parameter, N_t is the thermophoresis parameter, G_r is the local temperature Grashof number, B_r is the local nanoparticle Grashof number.

The flow equations for this model in dimensionless form under the assumptions of long wavelength and low Reynolds number after dropping the stars shall take the following forms

$$\frac{\partial p_m}{\partial x} = \frac{\partial^3 \psi}{\partial y^3} + R_e S^2 \frac{\partial^2 \Phi}{\partial y^2} + G_r \theta + B_r \Omega, \quad (14)$$
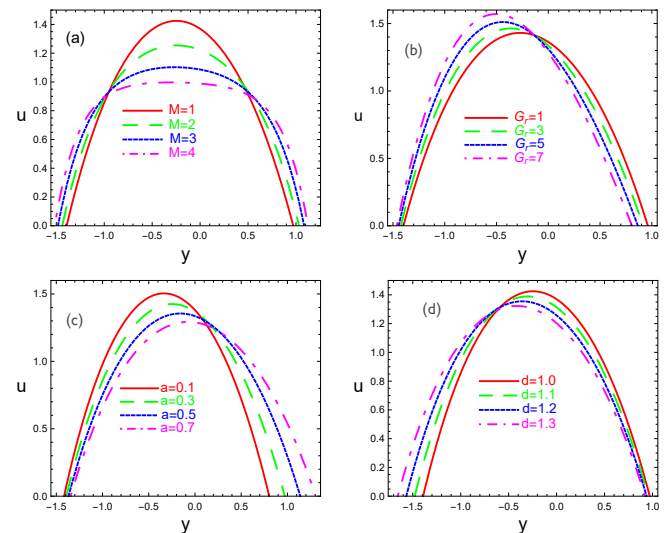
$$\frac{\partial p_m}{\partial y} = 0, \quad (15)$$

$$\frac{\partial^2 \theta}{\partial y^2} + N_b \frac{\partial \theta}{\partial y} \frac{\partial \Omega}{\partial y} + N_t (\frac{\partial \theta}{\partial y})^2 = 0, \quad (16)$$

$$\frac{\partial^2 \Omega}{\partial y^2} + \frac{N_t}{N_b} \frac{\partial^2 \theta}{\partial y^2} = 0, \quad (17)$$

$$E = \frac{\partial \psi}{\partial y} + \frac{1}{R_m} \frac{\partial^2 \Phi}{\partial y^2}. \quad (18)$$

Using (18) in (14) we get

$$\frac{\partial p_m}{\partial x} = \frac{\partial^3 \psi}{\partial y^3} + M^2 (E - \frac{\partial \psi}{\partial y}) + G_r \theta + B_r \Omega, \quad (19)$$

where $M^2 = R_e S^2 R_m$ is the Hartman number. Eliminating the pressure between (15) and (19) we get

$$\frac{\partial^4 \psi}{\partial y^4} - M^2 \frac{\partial \psi^2}{\partial y^2} + G_r \frac{\partial \theta}{\partial y} + B_r \frac{\partial \Omega}{\partial y} = 0, \quad (20)$$

The corresponding boundary conditions are

$$\psi = \frac{F}{2}, \quad \frac{\partial \psi}{\partial y} = -1, \quad \text{at} \quad y = h_1(x), \quad (21)$$
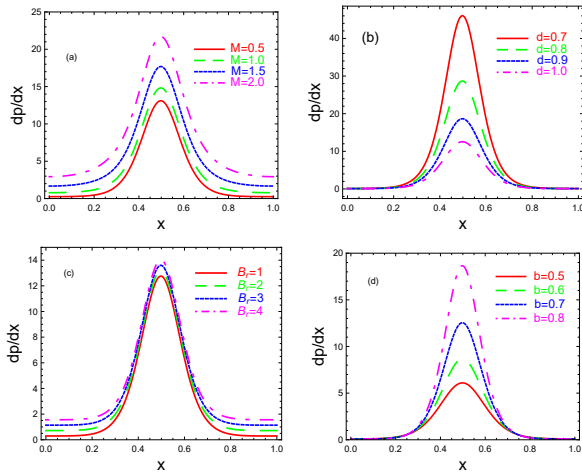
Fig. 3: Variations of the axial pressure gradient $\frac{dp}{dx}$ with x for various values of Hartmann number M (panel **a**), width of the channel k (panel **b**), local nanoparticles Grashof number B_r (panel **c**), amplitude of lower wave b (panel **d**). The other parameters chosen are: $F = -2, d = 1, a = 0.3, b = 0.7, N_b = 0.8, N_t = 0.5, \phi = 0.02, E = 0.1, y = 1, G_r = 0.5, B_r = 0.5$ (panel **a**); $F = -2, M = 0.1, a = 0.3, b = 0.7, N_b = 0.8, N_t = 0.5, \phi = 0.02, E = 0.1, y = 1, G_r = 0.5, B_r = 0.5$ (panel **b**); $F = -2, d = 1, a = 0.3, b = 0.7, N_b = 0.8, N_t = 0.5, \phi = 0.02, E = 0.1, y = 1, G_r = 0.5, M = 0.1$ (panel **c**); $F = -2, d = 1, a = 0.3, M = 0.1, N_b = 0.8, N_t = 0.5, \phi = 0.02, E = 0.1, y = 1, G_r = 0.5, B_r = 0.5$ (panel **d**).
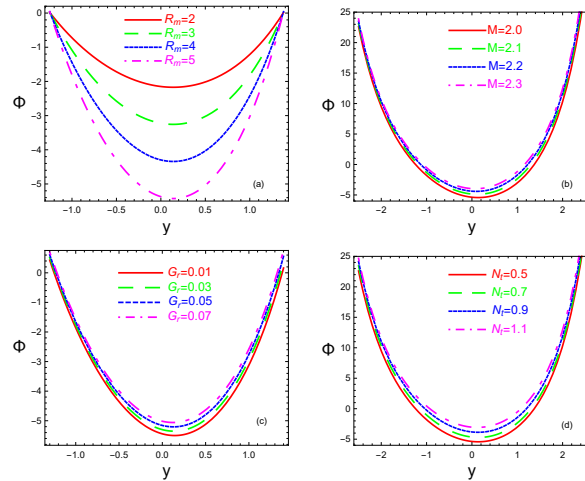

Fig. 5: Variations of magnetic force function Φ versus space variable y for different values of magnetic Reynolds number R_m (panel **a**), Hartmann number M (panel **b**), local temperature Grashof number Gr (panel **c**), and thermophoresis parameter N_t (panel **d**). The other parameters chosen are: $F = 6, d = 2, a = 0.7, b = 1.4, N_b = 0.8, N_t = 0.5, \phi = \frac{\pi}{2}, M = 2, G_r = 0.02, B_r = 1.5, E = 3.5$ (panel **a**); $F = 6, d = 2, a = 0.7, b = 1.4, N_b = 0.8, N_t = 0.5, \phi = \frac{\pi}{2}, R_m = 5, G_r = 0.02, B_r = 1.5, E = 3.5$ (panel **b**); $F = 6, d = 2, a = 0.7, b = 1.4, N_b = 0.8, N_t = 0.5, \phi = \frac{\pi}{2}, M = 2, R_m = 5, B_r = 1.5, E = 3.5$ (panel **c**); $F = 6, d = 2, a = 0.7, b = 1.4, N_b = 0.8, R_m = 5, \phi = \frac{\pi}{2}, M = 2, G_r = 0.02, B_r = 1.5, E = 3.5$ (panel **d**).
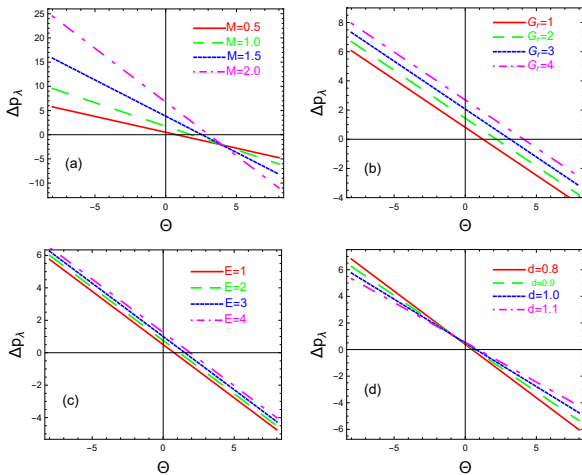

Fig. 6: Variations of axial induced magnetic field h_x against space variable y for different values magnetic Reynolds number R_m (panel **a**) and constant electric field E (panel **b**). The other parameters chosen are: $F = -3.5, d = 2.2, a = 0.7, b = 0.7, N_b = 0.8, N_t = 0.5, \phi = \pi, M = 3, G_r = 0.2, B_r = 1, E = 4$ (panel **a**); $F = -3.5, d = 2.2, a = 0.7, b = 0.7, N_b = 0.8, N_t = 0.5, \phi = \pi, M = 3, G_r = 0.2, B_r = 1, R_m = 2$ (panel **b**).

Fig. 4: Variations of dimensionless average rise in pressure ΔP_λ against Θ for various values of Hartmann number M (panel **a**), local temperature Grashof number Gr (panel **b**), constant electric field E (panel **c**), width of the channel d (panel **d**). The other parameters chosen are: $N_b = 0.8, N_t = 0.5, d = 1, a = 0.3, b = 0.7, G_r = 0.5, B_r = 0.5, \phi = \frac{\pi}{4}, E = 1$ (panel **a**); $N_b = 0.8, N_t = 0.5, d = 1, a = 0.3, b = 0.7, M = 0.5, B_r = 0.5, \phi = \frac{\pi}{4}, E = 1$ (panel **b**); $N_b = 0.8, N_t = 0.5, d = 1, a = 0.3, b = 0.7, G_r = 0.5, B_r = 0.5, \phi = \frac{\pi}{4}, M = 0.5$ (panel **c**); $N_b = 0.8, N_t = 0.5, M = 0.5, a = 0.3, b = 0.7, G_r = 0.5, B_r = 0.5, \phi = \frac{\pi}{4}, E = 1$ (panel **d**).
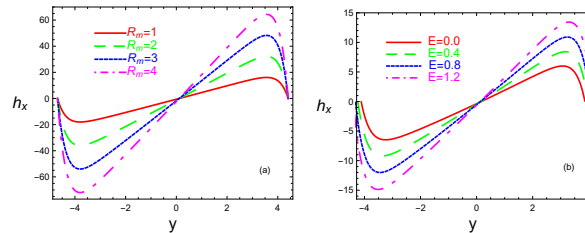
$$\psi = -\frac{F}{2}, \quad \frac{\partial \psi}{\partial y} = -1, \quad \text{at } y = h_2(x), \quad (22)$$

$$\theta = 0, \quad \Omega = 0, \quad \Phi = 0, \quad \text{at } y = h_1(x), \quad (23)$$

$$\theta = 1, \quad \Omega = 1, \quad \Phi = 0, \quad \text{at } y = h_2(x), \quad (24)$$
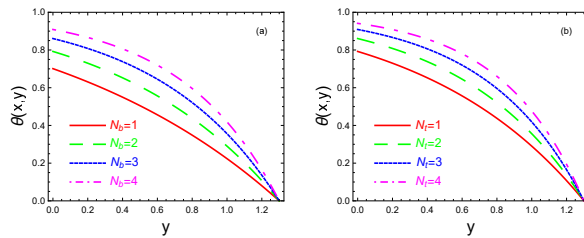
Fig. 7: Variations of local temperature of the fluid Θ with y for various values of Brownian motion parameter N_b (panel **a**), thermophoresis parameter N_t (panel **b**). The other parameters chosen are: $d = 1, a = 0.3, b = 0.5, N_t = 1, \phi = 0.2, x = 1$ (panel **a**); $d = 1, a = 0.3, b = 0.5, N_b = 2, \phi = 0.2, x = 1$ (panel **b**).
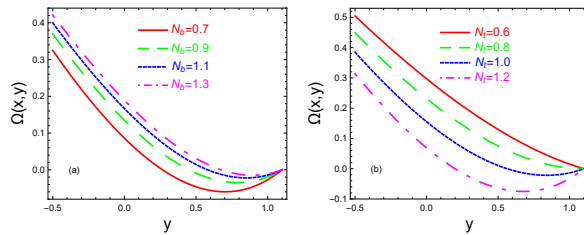

Fig. 8: Variations of nanoparticles concentration Ω with y for various values of Brownian motion parameter N_b (panel **a**), thermophoresis parameter N_t (panel **b**). The other parameters chosen are: $d = 1, a = 0.1, b = 0.5, N_t = 1.1, \phi = 0.2, x = 1$ (panel **a**); $d = 1, a = 0.3, b = 0.5, N_b = 0.8, \phi = 0.2, x = 1$ (panel **b**).
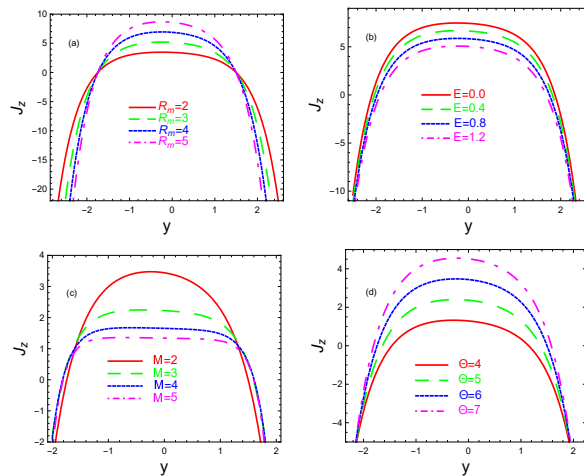

Fig. 9: Variations of the current density distribution J_z within y for different values of magnetic Reynolds number R_m (panel **a**), constant electric field E (panel **b**), Hartmann number M (panel **c**), and instantaneous volume flow rate Θ (panel **d**). The other parameters chosen are: $\Theta = 6, d = 1, a = 0.3, b = 0.7, N_b = 0.8, N_t = 0.5, \phi = \frac{\pi}{4}, M = 2, G_r = 0.02, B_r = 1, E = 2$ (panel **a**); $\Theta = 6, d = 1, a = 0.3, b = 0.7, N_b = 0.8, N_t = 0.5, \phi = \frac{\pi}{4}, M = 2, G_r = 0.02, B_r = 1, R_m = 2$ (panel **b**); $\Theta = 6, d = 1, a = 0.3, b = 0.7, N_b = 0.8, N_t = 0.5, \phi = \frac{\pi}{4}, R_m = 2, G_r = 0.02, B_r = 1, E = 2$ (panel **c**); $R_m = 2, d = 1, a = 0.3, b = 0.7, N_b = 0.8, N_t = 0.5, \phi = \frac{\pi}{4}, M = 2, G_r = 0.02, B_r = 1, E = 2$ (panel **d**).
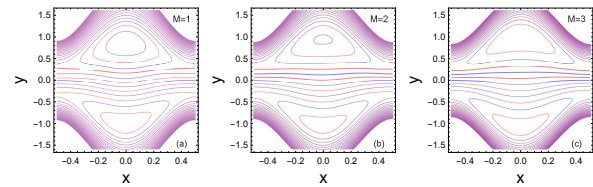

Fig. 10: Streamlines for three different values of Hartmann number M. The other parameters chosen are: $F = 0.2, d = 1, a = 0.5, b = 0.5, \phi = 0.02, N_b = 0.8, N_t = 0.5, G_r = 1, B_r = 0.5$.
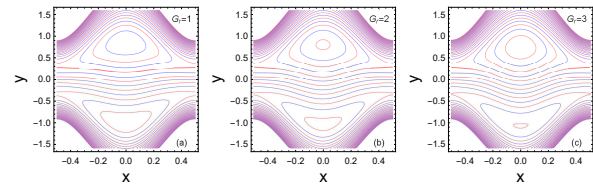

Fig. 11: Streamlines for three different values of local temperature Grashof number Gr. The other parameters chosen are: $F = 0.2, d = 1, a = 0.5, b = 0.5, \phi = 0.02, N_b = 0.8, N_t = 0.5, M = 1, B_r = 0.5$.

where,

$$h_1(x) = 1 + a\cos 2\pi x, \qquad h_2(x) = -d - b\cos(2\pi x + \phi). \tag{25}$$

3 Rate of volume flow

The volume flow rate in wave frame of reference is given by

$$q = \int_{h_2(x)}^{h_1(x)} u(x,y)dy, \tag{26}$$

where h_1, h_2 are functions of x alone.
The instantaneous volume flow rate in the fixed frame is given by

$$Q = \int_{H_2(x,t)}^{H_1(x,t)} [u(x,y,t) + c]dy = q + ch_1 - ch_2, \tag{27}$$

in which H_1, H_2 are functions of x and t.
The time-mean flow over time period $T = \lambda/c$ at a fixed position is given by

$$\bar{Q}(x,t) = \tfrac{1}{T}\int_0^T Q(x,y)dt = \tfrac{1}{T}\int_0^T (q + ch_1 - ch_2)dt = q + cd_1 + cd_2. \tag{28}$$

If we find the dimensionless mean flow Θ in the laboratory frame and F in the wave frame according to

$$\Theta = \frac{\bar{Q}}{cd_1}, \qquad F = \frac{q}{cd_1}, \tag{29}$$

one finds that Eq. (28) becomes

$$\Theta = F + 1 + d, \tag{30}$$

in which

$$F = \int_{h_2}^{h_1} u\,dy. \tag{31}$$

4 Closed form solution of the model

On integrating (17) twice with respect to y and then inserting the resulted equation into (16), we obtain

$$\frac{\partial^2 \theta}{\partial y^2} + N_b C_1(x)\frac{\partial \theta}{\partial y} = 0. \tag{32}$$

This equation can be exactly solved to give the temperature distribution, and hence the nanoparticles concentrations, as

$$\theta(x,y) = C_3(x) + C_4(x)e^{-N_b C_1(x)y}, \tag{33}$$

$$\Omega(x,y) = C_2(x) + C_1(x)y - \frac{N_t}{N_b}[C_3(x) + C_4(x)e^{-N_b C_1(x)y}], \tag{34}$$

where $C_i(x)$, $i = 1,2,3,4$ are unknown functions to be determined. On applying the boundary conditions (23, 24) on (33, 34), and then solving the resulted equations, we get

$$C_1(x) = \frac{N_b + N_t}{N_b(h_2 - h_1)}, \qquad C_2(x) = \frac{(N_b + N_t)h_1}{N_b(h_1 - h_2)}, \tag{35}$$

$$C_3(x) = \frac{e^{-N_b C_1(x)h_1}}{e^{-N_b C_1(x)h_1} - e^{-N_b C_1(x)h_2}},$$

$$C_4(x) = \frac{1}{e^{-N_b C_1(x)h_2} - e^{-N_b C_1(x)h_1}}. \tag{36}$$

On differentiating (33) and (34) with respect to y, then substituting in Eq.(20), we get

$$\Psi = A_1 + A_2 y + A_3 \cosh(My) + A_4 \sinh(My) + \frac{S_1 e^{S_2 y}}{S_2^2(S_2^2 - M^2)} - \frac{S_3 y^2}{2M^2} \tag{37}$$

where

$$S_1 = (G_r N_b - B_r N_t)C_1(x)C_4(x), \quad S_2 = -N_b C_1(x),$$
$$S_3 = -B_r C_1(x), \tag{38}$$

and the constants A_i, $i = 1,2,3,4$ are constants to be determined. On applying the boundary conditions (21, 22) on (37). (These constants can be easily obtained through using the Mathematica software). Substituting Eqs. (33), (34), and (37) into Eq. (19), we obtain that

$$\frac{\partial p_m}{\partial x} = \frac{S_1 e^{S_2 y}}{S_2} + S_3 y + G_r \theta + B_r \Omega + M^2(E - A_2). \tag{39}$$

The non dimensional pressure rise over one wavelength for the axial velocity is given by

$$\Delta P_\lambda = \int_0^1 (\frac{\partial P_m}{\partial x})\,dx. \tag{40}$$

The magnetic force function Φ can be obtained from (18) as follows

$$\Phi = \frac{1}{2}R_m E y^2 - R_m[\frac{1}{2}A_2 y^2 + \frac{1}{M}(A_3 \sinh[My] + A_4 \cosh[My]) + \frac{S_1 e^{S_2 y}}{S_2^3(S_2^2 - M^2)} - \frac{S_3 y^3}{6M^2}] + A_5 y + A_6. \tag{41}$$

where A_5, A_6 are constants can be determined by applying the boundary conditions (23) and (24). The axial induced magnetic field and current density are given by

$$h_x = \frac{\partial \Phi}{\partial y}, \qquad J_z = -\frac{\partial h_x}{\partial y} \tag{42}$$

Now we are in a position to discuss the results which we are obtained. This is seen in the next section.

5 Results and Discussion

To study the physical and graphical significance of various parameters on nanofluid flow in an asymmetric channel under the effects of induced magnetic field, Figs. (2)-(11) have been plotted. The effects of Hartmann number (M), local temperature Grashof number (Gr), amplitude of upper wave (a), and width of the channel (d) on the axial velocity can be observed through Fig. 2. It is clear from Fig. 2(a) that an increase in M causes decrease in magnitude of axial velocity U at the center of the channel for large values of M. From physical point of view this result is in accordance with the classical Hartmann result that "increasing the magnetic field strength led to decay in the velocity". Fig. 2(b) shows the influence of Gr on axial velocity distribution, it is observed that as Gr increases, the velocity increases in the region $y \in [-1.46, -0.149]$. An increasing in Gr means reducing the drag force and hence causes an increasing in the axial velocity. Fig. 2(c) depicts that the axial velocity decreases with an increase in the amplitude of upper wave a in the region $y \in [-1.42, 0.12]$ and increase in the rest of the region. The situation is completely opposite in Fig. 2(d), the axial velocity increases in the region $y \in [-1.65, -0.647]$ and decreases in the rest of the region with an increase in width of the channel d.

The pressure gradient for different values the Hartmann number M, width of the channel d, local nano particle Grashof number Br, and amplitude of lower wave b is plotted in Fig. 3. It had been founded that the magnitude of pressure gradient increases with an increase in M, Br, and b while it decreases if d is increased. It is also noticed that for $x \in [0, 0.3]$ and $x \in [0.7, 1]$ the

magnitude of pressure gradient is small. This leads to the fact that flow can easily pass in the middle of the channel. The effects of Hartmann number M, local temperature Grashof number Gr, constant electric field E, and width of the channel d on the dimensionless average rise in pressure ΔP_λ against the mean flow rate Θ are investigated in Fig. 4. The expression of pressure rise as shown in Eq. (52) is computed numerically by using MATHEMATICA software. This graph is divided to four regions as follows:
(i) The region $(\Theta > 0, \Delta P_\lambda > 0)$ refer to peristaltic pumping.
(ii) The region $(\Theta > 0, \Delta P_\lambda < 0)$ refer to augmented flow or copumping.
(iii) The region $(\Theta < 0, \Delta P_\lambda > 0)$ refer to retrograde or backward pumping.
(iv) The region $(\Theta < 0, \Delta P_\lambda < 0)$ refer to that the flow is reversed to focus of the peristaltic motion.

It is noticed that there is a linear relation between the average rise in pressure and the mean flow rate, also increasing Θ reduces the average rise in pressure, furthermore, in the peristaltic region, the maximum mean flow rate is achieved at zero average rise in pressure and the maximum average rise in pressure obtained at a zero mean flow rate. Fig. 4(a) shows the variation of ΔP_λ against Θ for various values of Hartmann number M. It is clear that an increase in M results in an increase of the peristaltic pumping, the free pumping $(\Delta P_\lambda = 0)$, and retrograde regions. Figs. 4(b, c) examine the variation of ΔP_λ against Θ for various values of local temperature Grashof number Gr and the constant electric field E. It is observed that increasing Gr and E led to an increase in peristaltic pumping rate and also an increase in the pressure rise. The variation of ΔP_λ versus Θ for different values of width of the channel d is presented in Fig. 4(d). It is obvious that the pressure rise increases in the peristaltic pumping and copumping regions, while it decreases in the retrograde region with an increase in d. The graphical results of the magnetic force function Φ versus space variable y for different values of magnetic Reynolds number R_m, Hartmann number M, local temperature Grashof number Gr, and thermophoresis parameter N_t are shown in Fig. 5. It is observed from Fig. 5(a) that the magnitude of magnetic force function increases with the increase in R_m. In Figs. 5(b) to 5(d) it is observed that with an increase in M, Gr, and N_t the magnitude of magnetic force function decreases.

The expressions for axial induced magnetic field h_x against space variable y for different values magnetic Reynolds number R_m and constant electric field E are displayed in Fig. 6. It is noticed that h_x and y are inversely proportional to each other if we increased R_m and E in the region $-4.4 < y < 0$, h_x decreases, while in the region $0 < y < 4.2$, h_x increases with an increase in R_m and E. Fig. 7 represents the effect of Brownian motion parameter N_b and thermophoresis parameter N_t on the local temperature of the fluid. It is clear that the local

temperature of the fluid increases when N_b and N_t are increased and this is in accordance with the conclusion that simultaneous increase in the Brownian motion parameter and thermophoresis parameter produces an increase in the temperature specially for sufficiently stronger thermophoresis effects.

The nanoparticles concentration profiles for different values of Brownian motion parameter N_b and thermophoresis parameter N_t are plotted in Fig. 8. It is obvious that increasing N_b led to an increase in the concentration of nanoparticles, while increasing N_t led to decrease the concentration of nanoparticles.

Figs. 9(a)-9(d) describe the current density distribution J_z within y for different values of magnetic Reynolds number R_m, constant electric field E, Hartmann number M, and Θ. It is noticed that magnitude of J_z near the center of the channel and decreases near the channel wall when R_m is increased (Fig. 9a). The situation is reversed in Fig. 9c, increasing M decreases J_z near the center of the channel and increases it near the channel wall. Also, E and instantaneous volume flow rate Θ have opposite effects on J_z, increasing E decreases J_z and increasing Θ led to an increase in J_z.

5.1 Trapping phenomenon

The trapping for different values of Hartmann number M and local temperature Grashof number G_r is shown in Figs. 10 and 11. It is seen from Fig. 10 that the size of trapping bolus increases by increasing M in the upper and lower parts of the channel while the number of the trapping bolus decreases only in the upper half of the channel. Fig. 11 presents that the size of trapping bolus decreases in the upper part of the channel and increases in the lower part with an increase in G_r.

6 Conclusions

In the present paper, the effect of induced magnetic field on peristaltic flow of a nanofluid in an asymmetric channel is studied. The problem is simplified under the assumptions of long wave length and low Reynolds number. Exact and closed form solutions of the problem have been presented. The results are discussed through graphs. The main findings are summarized as follows:
1- The magnitude of velocity decreases in the center of the channel and increases near the channel wall with an increase in M.
2- Axial pressure gradient increases with an increase in M, B_r, and b, while it decreases if d is increased.
3- The pressure rise increases with an increase in G_r and E.
4- The magnitude value of magnetic force function increases with an increase in R_m and decreases if M, G_r, and N_t are increased.

5- R_m and E have opposite effects on axial induced magnetic field.

6- Increasing N_b and N_t led to an increase in the local temperature of the fluid.

7- The concentration of nanoparticles increases by increasing N_b and decreases with an increase in N_t.

8- R_m and M have opposite influences on the current density distribution.

9- The number of trapped bolus decreases with an increase in M in the upper half of the channel.

10- The size of trapped bolus increases in the lower half of the channel by increasing M and G_r.

Acknowledgement

References

[1] S.U.S Choi, Enhancing thermal conductivity of fluids with nanoparticles. In: Siginer DA, Wang HP (eds) Developments and applications of Non-Newtonian flows, vol 66. ASME, New York, pp 99-105 (1995)

[2] K. Khanafer, K. Vafai , M. Lightstone, Buoyancy driven heat transfer enhancement in a two-dimensional enclosure utilizing nanofluids. Int.J.Heat Mass Transf. 46, 3639–3653 (2003)

[3] N. Putra, W. Roetzel, S.K. Das, Natural convection of nanofluids Heat Mass Transf., 39 (8), pp. 775-784 (2003)

[4] J. Koo, C. Kleinstreuer, Laminar nanofluid flow in microheat-sinks, Int. J. Heat Mass Transf., 48(13), pp. 2652-2661 (2005)

[5] Buongiorno J, Convective transport in nanofluids. ASME JHeat Transf 128:240-250 (2006)

[6] M. Ghazvini, H. Shokouhmand, Investigation of a nanofluid-cooled microchannel heat sink using Fin and porous media approaches Energy Convers. Manage., 50 (9), pp. 2373-2380 (2009)

[7] Khan WA, Pop I, Boundary-layer flow of a nanofluid past a stretching sheet. Int J Heat Mass Transf 53, 2477-2483 (2010)

[8] Y.M. Hung, Analytical study on forced convection of nanofluids with viscous dissipation in micro-channels Heat Transf. Eng., 31, pp. 1184-1192 (2010)

[9] D. Lelea, The performance evaluation of Al_2O_3/water nanofluid flow and heat transfer in micro-channel heat sink, Int. J. Heat Mass Transf., 54 (17), pp. 3891-3899 (2011)

[10] D. Lelea, C. Nisulescu, The micro-tube heat transfer and fluid flow of water based Al_2O_3 nanofluid with viscous dissipation, Int. Commun. Heat Mass Transf., 38 (6), pp.704-710 (2011)

[11] G. Huminic, A. Huminic, Numerical study on heat transfer characteristics of thermosyphon heat pipes using nanofluids, Energy Convers. Manage., 76, pp. 393-399 (2013)

[12] S. Akram, S. Nadeem, Consequence of nanofluid on peristaltic transport of a hyperbolic tangent fluid model in the occurrence of apt (tending) magnetic field, J. Magn. Magn. Mater., 358, pp. 183-191 (2014)

[13] N.S. Gad, Effect of Hall currents on interaction of pulsatile and peristaltic transport induced flows of a particlefluid suspension, Applied Mathematics and Computation 217, 4313-4320 (2011)

[14] E. Abo-Eldahab, E. Barakat, and Kh. Nowar, Hall Currents and Heat Transfer Effects on Peristaltic Transport in a Vertical Asymmetric Channel through a Porous Medium, Mathematical Problems in Engineering , Article ID 840203, Volume (2012) doi:10.1155/2012/840203

[15] Khalid Nowar, Peristaltic Flow of a Nanofluid under the Effect of Hall Current and Porous Medium, Mathematical Problems in Engineering , Article ID 389581, Volume (2014) http://dx.doi.org/10.1155/2014/389581

[16] F.M.Abbasi, T.Hayatb, A.Alsaedi, Numerical analysis for MHD peristaltic transport of Carreau Yasuda fluid in a curved channel with Hall effects, Journal of Magnetism and Magnetic Materials 382, 104-110 (2015)

[17] F.M. Abbasi, T. Hayat, B. Ahmad, Peristalsis of silver-water nanofluid in the presence of Hall and Ohmic heating effects: Applications in drug delivery, Journal of Molecular Liquids 207, 248-255 (2015)

[18] F.M.Abbasi, T.Hayatb, A.Alsaedi, Peristaltic transport of magneto-nanoparticles submerged in water: Model for drug delivery system Physica E 68, 123-132 (2015)

[19] Noreen Sher Akbar, M.Raza, R.Ellahi, Influence of induced magnetic field and heat flux with the suspension of carbon nanotubes for the peristaltic flow in a permeable channel, Journal of Magnetism and Magnetic Materials, 381, 405-415 (2015)

[20] Noreen Sher Akbar, Influence of magnetic field on peristaltic flow of a Casson fluid in an asymmetric channel: Application in crude oil refinement, Journal of Magnetism and Magnetic Materials, 378, 463-468 (2015)

[21] Vishnyakov, V. I. and Pavlov K. B., Peristaltic flow of a conductive liquid in a transverse magnetic field, Magnetohydroyanamics, 8 174-178 (1972)

[22] Kh.S. Mekheimer, Effect of induced magnetic field on peristaltic flow of a couple stress fluid, Physics Letters A 372, 4271-4278 (2008)

[23] Kh.S. Mekheimer, Peristaltic flow of a magneto-micropolar fluid: effect of induced magnetic field. J Appl Math, 23 p. Article ID 570825 (2008)

[24] Hayat T, Khan Y, Ali N, Mekheimer KhS, Effect of an induced magnetic field on the peristaltic flow of a third order fluid. Numer Methods Part Diff Equat, 26(2):345-66 (2010)

[25] T. Hayat, Najma Saleem, S. Asghar, Mohammed Shabab Alhothuali, Adnan Alhomaidan, Influence of induced magnetic field and heat transfer on peristaltic transport of a Carreau fluid, Commun Nonlinear Sci Numer Simulat 16, 3559-3577 (2011)

[26] Y. Abd elmaboud, Influence of induced magnetic field on peristaltic flow in an annulus, Commun Nonlinear Sci Numer Simulat 17, 685-698 (2012)

[27] Safia Akram, S.Nadeem, M. Hanif, Numerical and analytical treatment on peristaltic flow of Williamson fluid in the occurrence of induced magnetic field , Journal of Magnetism and Magnetic Materials, 346, 142-151 (2013)

[28] Safia Akram, S.Nadeem, Influence of induced magnetic field and heat transfer on the peristaltic motion of a Jeffrey fluid in an asymmetric channel: Closed form solutions, Journal of Magnetism and Magnetic Materials, 328, 11-20 (2013)

[29] M. Mustafa, S. Hina, T. Hayat, B. Ahmad, Influence of induced magnetic field on the peristaltic flow of nanofluid, Meccanica, 49:521-534 (2014)

Khalid Nowar He received Bachelor of Science in 1998 from Mathematics Department, Zagazig University (Banha branch), Egypt. He received the M.Sc. degree in 2007 from Mathematics Department, Faculty of Science, Tanta University, Egypt. He received the Ph.D. degree in 2012 from Mathematics Department, Faculty of Science, Helwan University, Egypt. He had been employed as a demonstrator at 15th may Higher Institute of engineering from Dec. 2007 to Sep 2009. He is working as a lecturer at Mathematics department, College of Science, King Saud University (Saudi Arabia) from Oct. 2009 up till now. His research area of interest lies in the branches of applied mathematics and mathematical physics especially including the mathematical methods and models which describe uid mechanics and its applications.